Progress In Electromagnetics Research B, Vol. 4, 249–261, 2008

NEAR-FIELD — FAR-FIELD TRANSFORMATION TECHNIQUE WITH HELICOIDAL SCANNING FOR ELONGATED ANTENNAS

F. D'Agostino, F. Ferrara, C. Gennarelli, R. Guerriero and M. Migliozzi

Dipartimento di Ingegneria dell'Informazione ed Ingegneria Elettrica
University of Salerno, via Ponte Don Melillo
Fisciano 84084, Salerno, Italy

Abstract—A fast and accurate near-field — far-field transformation technique with helicoidal scanning is proposed in this paper. It is tailored for elongated antennas, since a prolate ellipsoid instead of a sphere is considered as surface enclosing the antenna under test. Such an ellipsoidal modelling allows one to consider measurement cylinders with a diameter smaller than the antenna height, thus reducing the error related to the truncation of the scanning surface. Moreover, it is quite general, containing the spherical modelling as particular case, and allows a significant reduction of the number of the required near-field data when dealing with elongated antennas. Numerical tests are reported for demonstrating the accuracy of the far-field reconstruction process and its stability with respect to random errors affecting the data.

1. INTRODUCTION

The time needed for collecting the near-field data can be remarkably reduced by means of continuous movements of the positioning systems of the probe and antenna under test (AUT), as suggested by Rahmat-Samii et al. in [1]. By following this suggestion, innovative near-field — far-field (NF-FF) transformation techniques from a nonredundant number of data acquired along spirals wrapping the conventional scanning surfaces have been recently developed [2–7]. In particular, a NF-FF transformation with helicoidal scanning (Fig. 1) has been proposed in [2, 3], a planar spiral arrangement of samples has been considered in [4], and a NF-FF transformation with spherical spiral scanning has been developed in [5, 6].

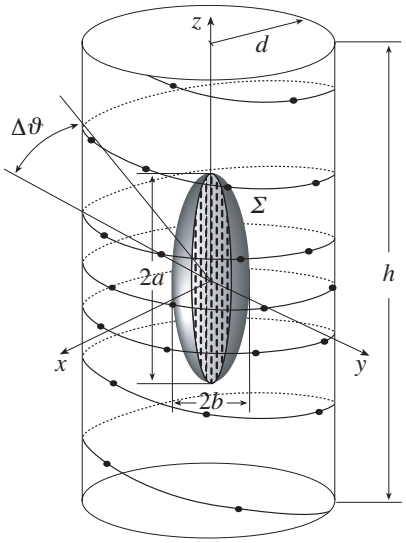

Figure 1. Helicoidal scanning.

In all the cases, efficient two-dimensional interpolation formulas for recovering the NF data required by the NF-FF transformations employing the conventional scannings [8] have been obtained by applying the theoretical results on the nonredundant sampling representations of electromagnetic (EM) fields [9] and assuming the AUT enclosed in a ball of radius a. This target has been achieved: a) by developing a nonredundant sampling representation of the voltage on the considered curve (helix or spiral); b) by choosing the step of such a curve equal to the sample spacing required to interpolate the data along the corresponding meridian curve (generatrix, radial line, and meridian). Moreover, a unified theory of the spiral scannings has been provided in [7]. In fact, it has been proved that the voltage acquired by a nondirective probe can be reconstructed on a quite arbitrary rotational surface from a nonredundant number of its samples lying on a proper spiral wrapping it. This surface is obtained by rotating a meridian curve always external to the cone tangent to the sphere modelling the AUT and having the vertex at the observation point. The proof has been attained by revisiting the approach in [9] to obtain the optimal phase function to extract from the voltage expression and the parameter to be used for describing the scanning curve. It is worth noting that the voltage can be determined by using the same interpolation scheme, even if the spiral lies on geometrically different surfaces.

However, the use of the spherical AUT modelling prevents the possibility of considering measurement cylinders (planes) with a radius (distance) smaller than one half the source maximum size. This drawback occurs in the helicoidal and in the planar spiral scannings when considering elongated and quasi-planar antennas, respectively. Obviously, this reflects in an increase of the error related to the truncation of the scanning surface. In fact, for a given size of the scan zone, such an error raises on increasing the distance. Moreover, the volumetric redundancy of the spherical modelling gives rise to an increase in the number of the NF data, when the AUT geometry departs from the spherical one.

The aim of this paper is to develop an efficient NF-FF transformation technique with helicoidal scanning tailored for elongated antennas, which allows to overcome the abovementioned drawbacks. To this end, the AUT is considered as enclosed in a prolate spheroid (Fig. 1), a shape particularly suitable to deal with such a kind of antennas, but which remains quite general and contains the spherical modelling as particular case.

2. THE SPHERICAL MODELLING OF THE ANTENNA

Let us consider a non directive probe which scans a helix with constant angular step lying on a cylinder of radius d surrounding the AUT (see Fig. 1) and adopt the spherical coordinate system (r, ϑ, φ) for denoting the observation point P in the NF region. Since the voltage V measured by this kind of probe has the same effective spatial bandwidth of the field, the theoretical results on the nonredundant representation of EM fields [9] can be applied to such a voltage. Accordingly, if the AUT is enclosed in a sphere of radius a (AUT ball) and the helix is described by a proper analytical parameterization $\underline{r} = \underline{r}(\xi)$, the probe "reduced voltage"

$$\tilde{V}(\xi) = V(\xi)e^{j\gamma(\xi)} \tag{1}$$

can be closely approximated by a spatially bandlimited function, $\gamma(\xi)$ being a phase function to be determined. The related bandlimitation error becomes negligible as the bandwidth exceeds a critical value W_ξ [9], so that it can be effectively controlled by choosing a bandwidth equal to $\chi' W_\xi$, wherein the excess bandwidth factor χ' is slightly greater than unity for an electrically large AUT.

To obtain a sampling representation of the voltage on the cylinder from its nonredundant samples collected along a helix with constant angular step, it is necessary: a) to develop a nonredundant voltage representation on the helix; b) to choose the helix step equal to the

sample spacing needed to interpolate the voltage along a cylinder generatrix.

The parametric equations of the helix, when imposing its passage through a fixed point Q_0 of the generatrix at $\varphi = 0$, are: $x = d\cos(\phi - \phi_i)$, $y = d\sin(\phi - \phi_i)$, $z = d\cot\theta$, where ϕ is the angular parameter describing the helix, ϕ_i is the value of ϕ at Q_0, and $\theta = k\phi$. The parameter k is such that the angular step, determined by the consecutive intersections $Q(\phi)$ and $Q(\phi + 2\pi)$ with a generatrix, is $\Delta\theta = 2\pi k$. It is worth noting that the helix can be obtained by radially projecting on the measurement cylinder the spiral wrapping the AUT ball with the same angular step.

As shown in [7], a nonredundant sampling representation of the voltage on the helix can be obtained by using the following expressions for the optimal phase function and parameterization:

$$\gamma = \beta \int_0^r \sqrt{1 - a^2/r'^2}\, dr' = \beta\sqrt{r^2 - a^2} - \beta a \cos^{-1}\left(\frac{a}{r}\right) \tag{2}$$

$$\xi = \frac{\beta a}{W_\xi} \int_0^\phi \sqrt{k^2 + \sin^2 k\phi'}\, d\phi' \tag{3}$$

where β is the wavenumber.

Since the elevation step of the helix must be equal to the sample spacing required for the interpolation along a generatrix, then, according to [9], $\Delta\theta = \Delta\vartheta = 2\pi/(2N'' + 1)$, with $N'' = \mathrm{Int}(\chi N') + 1$ and $N' = \mathrm{Int}(\chi'\beta a) + 1$, $\chi > 1$ being an oversampling factor. As a consequence, $k = 1/(2N'' + 1)$.

According to (3), ξ is proportional to the curvilinear abscissa along the spiral wrapping the sphere modelling the source. Since such a spiral is a closed curve, it is convenient to choose the bandwidth W_ξ such that ξ covers a 2π range when the whole curve on the sphere is described. As a consequence,

$$W_\xi = \frac{\beta a}{\pi} \int_0^{(2N''+1)\pi} \sqrt{k^2 + \sin^2 k\phi'}\, d\phi' \tag{4}$$

According to these results, the optimal sampling interpolation (OSI) formula of central type to reconstruct the voltage at any point Q of the helix is [7, 9]:

$$\tilde{V}(\xi) = \sum_{m=m_0-p+1}^{m_0+p} \tilde{V}(\xi_m)\, \Omega_M(\xi - \xi_m)\, D_{M''}(\xi - \xi_m) \tag{5}$$

where $m_0 = \mathrm{Int}[(\xi - \xi(\phi_i))/\Delta\xi]$ is the index of the sample nearest (on the left) to the output point, $2p$ is the number of retained samples $\tilde{V}(\xi_m)$, and

$$\xi_m = \xi(\phi_i) + m\Delta\xi = \xi(\phi_i) + 2\pi m/\left(2M'' + 1\right) \tag{6}$$

with $M'' = \mathrm{Int}(\chi M') + 1$ and $M' = \mathrm{Int}(\chi' W_\xi) + 1$. Moreover,

$$\begin{aligned} D_{M''}(\xi) &= \frac{\sin\left((2M''+1)\,\xi/2\right)}{(2M''+1)\sin(\xi/2)}; \\ \Omega_M(\xi) &= \frac{T_M\left[-1 + 2\left(\cos(\xi/2)/\cos\left(\bar{\xi}/2\right)\right)^2\right]}{T_M[-1 + 2/\cos^2\left(\bar{\xi}/2\right)]} \end{aligned} \tag{7}$$

are the Dirichlet and Tschebyscheff Sampling functions, wherein $T_M(\xi)$ is the Tschebyscheff polynomial of degree $M = M'' - M'$ and $\bar{\xi} = p\Delta\xi$.

The OSI formula (5) can be used to evaluate the "intermediate samples", namely, the voltage values at the intersection points between the helix and the generatrix passing through P. Once these samples have been evaluated, the voltage at P can be reconstructed via the following OSI expansion:

$$\tilde{V}(\vartheta, \varphi) = \sum_{n=n_0-q+1}^{n_0+q} \tilde{V}\left(\vartheta_n\right) \Omega_N\left(\vartheta - \vartheta_n\right) D_{N''}\left(\vartheta - \vartheta_n\right) \tag{8}$$

where $N = N'' - N'$, $n_0 = \mathrm{Int}[(\vartheta - \vartheta_0)/\Delta\vartheta]$, $2q$ is the number of the retained intermediate samples $\tilde{V}(\vartheta_n)$, and

$$\vartheta_n = \vartheta_n(\varphi) = \vartheta\left(\phi_i\right) + k\varphi + n\Delta\vartheta = \vartheta_0 + n\Delta\vartheta \tag{9}$$

The described two-dimensional OSI algorithm can be properly applied to recover the NF data required by the NF–FF transformation technique [10].

3. THE PROLATE ELLIPSOIDAL MODELLING OF THE ANTENNA

As already stated, the use of the spherical modelling of the AUT does not allow to consider scanning cylinder having diameter less than the antenna maximum size. This is a serious drawback when dealing with elongated antennas. In fact, for a given height of the measurement cylinder, the error related to the truncation of the scanning zone raises on increasing the radius of the cylinder. Moreover, the volumetric

redundancy of the spherical modelling gives rise to a useless increase in the number of NF data, when the AUT geometry departs from the spherical one. To overcome these drawbacks, the previously described sampling representation will be properly extended in this Section to the case of elongated antennas.

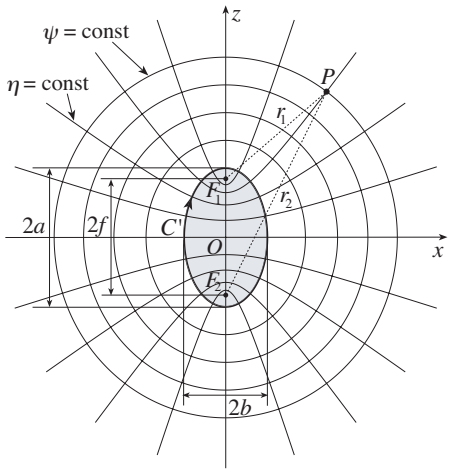

Figure 2. Ellipsoidal source modelling.

An effective modelling for this kind of antennas is obtained by considering them as enclosed in the smallest prolate ellipsoid having major and minor semi-axes equal to a and b (see Fig. 2). In such a case, by adopting $W_\eta = \beta\ell'/2\pi$ (ℓ' being the length of the intersection curve C' between the meridian plane through P and the ellipsoid), the optimal expressions for the phase function ψ and the parameterization η to be used for describing a cylinder generatrix become [9]:

$$\psi = \beta a \left[v\sqrt{\frac{(v^2-1)}{(v^2-\varepsilon^2)}} - E\left(\cos^{-1}\sqrt{\frac{(1-\varepsilon^2)}{(v^2-\varepsilon^2)}}|\varepsilon^2\right)\right] \tag{10}$$

$$\eta = (\pi/2)\left[1 + E\left(\sin^{-1}u|\varepsilon^2\right)/E\left(\pi/2|\varepsilon^2\right)\right] \tag{11}$$

where $u = (r_1 - r_2)/2f$ and $v = (r_1 + r_2)/2a$ are the elliptic coordinates, $r_{1,2}$ being the distances from P to the foci and $2f$ the focal distance of C'. Moreover, $\varepsilon = f/a$ is the eccentricity of C', and $E(\cdot|\cdot)$ denotes the elliptic integral of second kind. It is worth noting that in any meridian plane the curves $\psi = \text{const}$ and $\eta = \text{const}$ are ellipses and hyperbolas confocal to C' (Fig. 2), instead of circumferences and radial lines.

According to a heuristic reasoning, the helix can be again obtained by projecting a spiral wrapping the ellipsoid modelling the AUT on

the scanning cylinder. The elevation step of such a spiral is equal to the sample spacing $\Delta\eta$ needed for the voltage interpolation along a generatrix. The projection is now obtained by means of the hyperbolas at $\eta = \text{const}$, that in the case of spheroidal source modelling take the role of the radial lines of the spherical one. Accordingly, the parametric equations of the helix become:

$$\begin{cases} x = d\cos(\phi - \phi_i) \\ y = d\sin(\phi - \phi_i) \\ z = d\cot[\theta(\eta)] \end{cases} \tag{12}$$

wherein $\eta = k\phi = \phi/(2N'' + 1)$.

A quite analogous reasoning allows one to determine the phase function and the parameterization to be used for obtaining a nonredundant sampling representation along the helix. In particular, by generalizing relations (2) and (3), the phase function γ coincides with ψ defined in (10) and the parameter ξ is β/W_ξ times the curvilinear abscissa of the projecting point that lies on the spiral wrapping the ellipsoid. Moreover, according to (4), W_ξ is chosen to be equal to β/π times the length of the spiral wrapping the ellipsoid from pole to pole. As a conclusion, the spiral, γ and ξ are such that they coincide with those relevant to the spherical modelling when the prolate ellipsoid approaches to a sphere.

It is worthy to note that the OSI formula (5) can be still used to reconstruct the reduced voltage at any point on the helix and, as a consequence, can be applied to recover the intermediate samples, whereas the NF data required to carry out the NF-FF transformation [10] can be reconstructed by means of the following OSI expansion:

$$\tilde{V}(\eta(\vartheta), \varphi) = \sum_{n=n_0-q+1}^{n_0+q} \tilde{V}(\eta_n)\, \Omega_N(\eta - \eta_n)\, D_{N''}(\eta - \eta_n) \tag{13}$$

wherein $N = N'' - N'$, $N' = \text{Int}(\chi' W_\eta) + 1$, $n_0 = \text{Int}[(\eta - \eta_0)/\Delta\eta]$, $2q$ is the number of the retained intermediate samples $\tilde{V}(\eta_n)$, and

$$\eta_n = \eta_n(\varphi) = \eta(\phi_i) + k\varphi + n\Delta\eta = \eta_0 + n\Delta\eta \tag{14}$$

4. NF-FF TRANSFORMATION

For reader's convenience, the key steps of the standard probe compensated NF-FF transformation technique with cylindrical scanning [10] are reported. According to such a technique, the modal

coefficients a_ν and b_ν of the cylindrical wave expansion of the field radiated by the AUT are related to: i) the two-dimensional Fourier transforms I_ν and I'_ν of the output voltage of the probe for two independent sets of measurements (the probe is rotated 90° about its longitudinal axis in the second set); ii) the coefficients c_m, d_m and c'_m, d'_m of the cylindrical wave expansion of the field radiated by the probe and the rotated probe, respectively, when used as transmitting antennas. The key relations are:

$$\begin{aligned} a_\nu(\alpha) &= \frac{\beta^2}{\Lambda^2 \Delta_\nu(\alpha)} \left[I_\nu(\alpha) \sum_{m=-\infty}^{\infty} d'_m(-\alpha) H^{(2)}_{\nu+m}(\Lambda d) \right. \\ &\quad \left. - I'_\nu(\alpha) \sum_{m=-\infty}^{\infty} d_m(-\alpha) H^{(2)}_{\nu+m}(\Lambda d) \right] \end{aligned} \tag{15}$$

$$\begin{aligned} b_\nu(\alpha) &= \frac{\beta^2}{\Lambda^2 \Delta_\nu(\alpha)} \left[I'_\nu(\alpha) \sum_{m=-\infty}^{\infty} c_m(-\alpha) H^{(2)}_{\nu+m}(\Lambda d) \right. \\ &\quad \left. - I_\nu(\alpha) \sum_{m=-\infty}^{\infty} c'_m(-\alpha) H^{(2)}_{\nu+m}(\Lambda d) \right] \end{aligned} \tag{16}$$

$$\begin{aligned} I_\nu(\alpha) &= \int_{-\infty}^{\infty} \int_{-\pi}^{\pi} V(\varphi, z) e^{-j\nu\varphi} e^{j\alpha z} d\varphi dz; \\ I'_\nu(\alpha) &= \int_{-\infty}^{\infty} \int_{-\pi}^{\pi} V'(\varphi, z) e^{-j\nu\varphi} e^{j\alpha z} d\varphi dz \end{aligned} \tag{17}$$

$$\begin{aligned} \Delta_\nu(\alpha) = &\sum_{m=-\infty}^{\infty} c_m(-\alpha) H^{(2)}_{\nu+m}(\Lambda d) \sum_{m=-\infty}^{\infty} d'_m(-\alpha) H^{(2)}_{\nu+m}(\Lambda d) \\ &- \sum_{m=-\infty}^{\infty} c'_m(-\alpha) H^{(2)}_{\nu+m}(\Lambda d) \sum_{m=-\infty}^{\infty} d_m(-\alpha) H^{(2)}_{\nu+m}(\Lambda d) \end{aligned} \tag{18}$$

where $\Lambda = \sqrt{\beta^2 - \alpha^2}$, $H^{(2)}_\nu(\cdot)$ is the Hankel function of second kind and order ν, and V, V' represent the output voltage of the probe and the rotated probe at the point (d, φ, z).

Once the modal coefficients have been determined, the FF components of the electric field in the spherical coordinate system

(R, Θ, Φ) can be evaluated by:

$$E_\Theta(R,\Theta,\Phi) = -j2\beta\frac{e^{-j\beta R}}{R}\sin\Theta\sum_{\nu=-\infty}^{\infty} j^\nu b_\nu(\beta\cos\Theta)e^{j\nu\Phi} \quad (19)$$

$$E_\Phi(R,\Theta,\Phi) = -2\beta\frac{e^{-j\beta R}}{R}\sin\Theta\sum_{\nu=-\infty}^{\infty} j^\nu a_\nu(\beta\cos\Theta)e^{j\nu\Phi} \quad (20)$$

5. NUMERICAL TESTS

Some numerical tests assessing the effectiveness of the developed technique are reported in the following. The first simulation refers to a uniform planar array (Fig. 1) of elementary Huygens sources polarized along the z axis. Its elements cover an elliptical zone in the plane $y = 0$, with major and minor semi-axes equal to 30λ and 6λ, and are spaced by 0.4λ along x and 0.6λ along z, λ being the wavelength. An open-ended WR-90 rectangular waveguide, operating at the frequency of 10 GHz, is chosen as probe. The NF data are collected on a helix wrapping a cylinder with radius $d = 12\lambda$ and height $h = 180\lambda$.

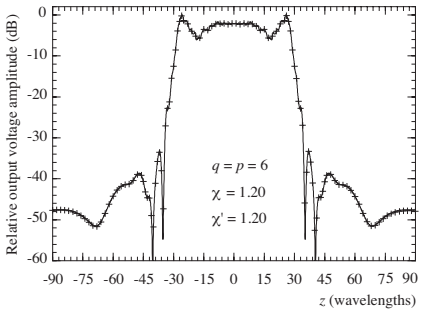

Figure 3. Amplitude of V on the generatrix at $\varphi = 90°$. Solid line: exact. Crosses: interpolated.

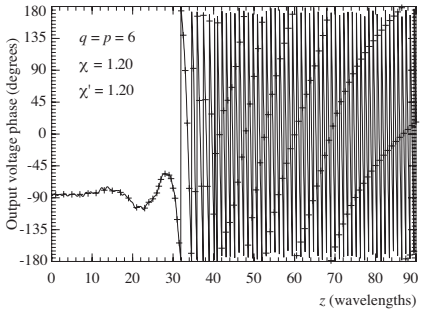

Figure 4. Phase of V on the generatrix at $\varphi = 90°$. Solid line: exact. Crosses: interpolated.

Figures 3 and 4 show the reconstruction of the amplitude and phase of the output voltage V on the generatrix at $\varphi = 90°$. As can be seen, there is an excellent agreement between the exact voltage and the reconstructed one. The accuracy is also confirmed by the values of the maximum and mean-square errors (normalized to the voltage maximum value on the cylinder) reported in Figs. 5 and 6, respectively. They have been obtained by comparing the interpolated values of V

with those directly evaluated on a close grid in the central zone of the cylinder, so that the existence of the guard samples is assured. As expected, the errors decrease up to very low values on increasing the oversampling factor and/or the number of the retained samples. The algorithm stability has been investigated by adding random errors to the exact samples. These errors simulate a background noise, bounded to Δa in amplitude and with arbitrary phase, and uncertainties on the data of $\pm\Delta a_r$ in amplitude and $\pm\Delta\sigma$ in phase. As shown in Fig. 7, the interpolation algorithm works well also when dealing with error affected data. The reconstructions of the antenna FF pattern in the principal planes are shown in Figs. 8 and 9. As can be seen, the exact and recovered fields are practically indistinguishable, thus assessing

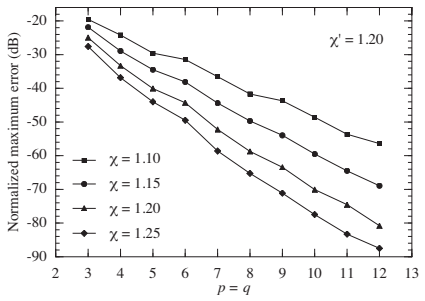

Figure 5. Normalized maximum reconstruction error.

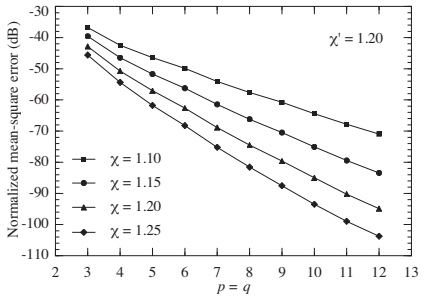

Figure 6. Normalized mean-square reconstruction error.

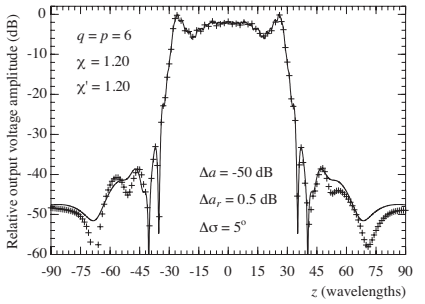

Figure 7. Amplitude of V on the generatrix at $\varphi = 90°$. Solid line: exact. Crosses: interpolated from error affected data.

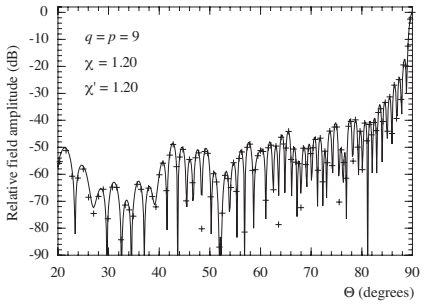

Figure 8. E-plane pattern. Solid line: exact. Crosses: reconstructed from NF measurements.

the effectiveness of the developed NF–FF transformation technique.

Note that the number of the samples employed for reconstructing the NF data over the considered cylinder is 15153 (guard samples included), significantly less than that (46080) required by the approach in [11].

As already stated, the use of the spherical AUT modelling prevents the possibility of considering measurement cylinders with a radius smaller than one half the antenna maximum size, thus giving rise to an increase of the truncation error for a given size of the scanning zone. In order to highlight this drawback, another reconstruction of the E-plane pattern, obtained by employing the spherical modelling, is shown in Fig. 10. In such a case, the NF data have been collected on a helix that covers a cylinder having the same height but radius of 36 λ. As can be clearly seen, the reconstruction is less accurate in the far out side lobe region.

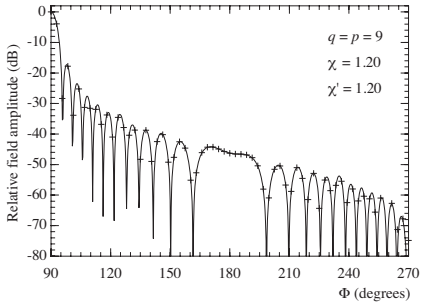

Figure 9. H-plane pattern. Solid line: exact. Crosses: reconstructed from NF measurements.

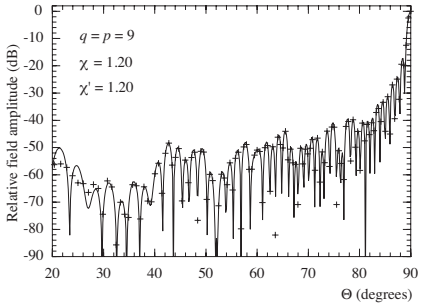

Figure 10. E-plane pattern. Solid line: exact. Crosses: reconstructed from NF measurements when using the spherical modelling.

At last, in order to test the algorithm performances in a more severe condition, a further example is considered in the following. It refers to a planar Tschebyscheff array with sidelobe ratio (SLR) equal to 40 dB. Its elements, elementary Huygens sources linearly polarized along z, are $\lambda/2$ spaced and cover a $6\lambda \times 51\lambda$ rectangle in the xz-plane. The radius and the height of the scanning cylinder, and the semi-axes of the prolate ellipsoid modelling the AUT are the same as in the first example. The corresponding FF pattern in the E-plane is reported in Fig. 11. Also in this case, the FF reconstruction results to be very accurate.

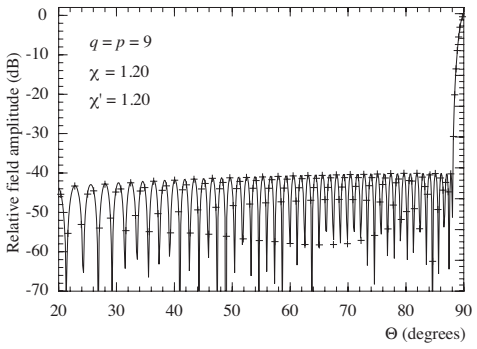

Figure 11. *E*-plane pattern of a Tschebyscheff array. Solid line: exact. Crosses: reconstructed from NF measurements.

6. CONCLUSIONS

An innovative NF-FF transformation with helicoidal scanning has been developed in this paper by using an ellipsoidal modelling of the source, instead of the previously adopted spherical one. Such a modelling, tailored for elongated antennas, allows one to consider measurement cylinders with a diameter smaller than the antenna height, thus reducing the error related to the truncation of the scanning surface. Moreover, it contains the spherical modelling as particular case and lowers significantly the number of required data when dealing with elongated antennas. The reported numerical examples have demonstrated the accuracy of the technique and its stability with respect to random errors affecting the NF data.

REFERENCES

1. Yaccarino, R. G., L. I. Williams, and Y. Rahmat-Samii, "Linear spiral sampling for the bipolar planar antenna measurement technique," *IEEE Trans. Antennas Propagat.*, Vol. 44, 1049–1051, July 1996.
2. Bucci, O. M., C. Gennarelli, G. Riccio, and C. Savarese, "Probe compensated NF-FF transformation with helicoidal scanning," *Journal of Electromagnetic Waves and Applications*, Vol. 14, 531–549, 2000.
3. Bucci, O. M., C. Gennarelli, G. Riccio, and C. Savarese, "Nonredundant NF-FF transformation with helicoidal scanning," *Journal of Electromagnetic Waves and Applications*, Vol. 15, No. 11, 1507–1519, 2001.

4. Bucci, O. M., F. D'Agostino, C. Gennarelli, G. Riccio, and C. Savarese, "Probe compensated FF reconstruction by NF planar spiral scanning," *IEE Proc. Microw., Ant. Prop.*, Vol. 149, 119–123, April 2002.
5. Bucci, O. M., F. D'Agostino, C. Gennarelli, G. Riccio, and C. Savarese, "NF-FF transformation with spherical spiral scanning," *IEEE Antennas Wireless Propagat. Lett.*, Vol. 2, 263–266, 2003.
6. D'Agostino, F., F. Ferrara, C. Gennarelli, G. Riccio, and C. Savarese, "Directivity computation by spherical spiral scanning in NF region," *Journal of Electromagnetic Waves and Applications*, Vol. 19, 1343–1358, 2005.
7. D'Agostino, F., C. Gennarelli, G. Riccio, and C. Savarese, "Theoretical foundations of near-field — far-field transformations with spiral scannings," *Progress In Electromagnetics Research*, PIER 61, 193–214, 2006.
8. Gennarelli, C., G. Riccio, F. D'Agostino, and F. Ferrara, *Near-field — Far-field Transformation Techniques*, Vol. 1, CUES, Salerno, Italy, 2004.
9. Bucci, O. M., C. Gennarelli, and C. Savarese, "Representation of electromagnetic fields over arbitrary surfaces by a finite and nonredundant number of samples," *IEEE Trans. Antennas Propagat.*, Vol. 46, 351–359, March 1998.
10. Leach, W. M., Jr. and D. T. Paris, "Probe compensated NF measurements on a cylinder," *IEEE Trans. Antennas Propagat.*, Vol. 21, 435–445, July 1973.
11. Costanzo, S. and G. Di Massa, "Far-field reconstruction from phaseless near-field data on a cylindrical helix," *Journal of Electromagnetic Waves and Applications*, Vol. 18, No. 8, 1057–1071, 2004.